$AA'_2Rh_6O_{12}$: A New Family of Rhodium Oxides Exhibiting High Thermopower Coupled with High Electrical Conductivity

Hiroshi Mizoguchi,[†] L. N. Zakharov,[†] W. J. Marshall,[‡] A. W. Sleight,[†] and M. A. Subramanian*,[†]

Department of Chemistry and OSUMI, Oregon State University, Corvallis, Oregon 97331-4003, and DuPont Central Research and Development, Experimental Station, Wilmington, Delaware 19880

Received December 11, 2008. Revised Manuscript Received January 22, 2009

A new family of rhodium oxides with the $SrCa_2Sc_6O_{12}$ structure has been discovered. The new compounds prepared are $SrMg_2Rh_6O_{12}$, $La_{1-x}Mg_{2-y}Rh_6O_{12}$, $Bi_{0.78}Li_2Rh_6O_{12}$, $Pb_{0.78}Li_2Rh_6O_{12}$, $Bi_{0.75}Sc_{1.10}(Rh_{4.92}Sc_{1.08})O_{12}$, $SrBe_2Rh_6O_{12}$, and $Bi_{0.68}Be_2Rh_6O_{12}$. All compounds can be considered Rh^{3+}/Rh^{4+} mixed-valence compounds with the highest average oxidation being +3.4. Structural analyses based on single-crystal X-ray diffraction data were performed for four of the compounds, and triangular coordination for Be was found in the case of $Bi_{0.68}Be_2Rh_6O_{12}$. All the compounds are good electrical conductors, and a Seebeck coefficient of 200 μV/K was found for $Bi_{0.78}Li_2Rh_6O_{12}$ and $SrMg_2Rh_6O_{12}$. The magnetic properties of $Pb_{0.78}Li_2Rh_6O_{12}$, $Bi_{0.78}Li_2Rh_6O_{12}$ and $Bi_{0.68}Be_2Rh_6O_{12}$ are discussed.

Introduction

Recently, cobalt-containing oxides (e.g., Na_xCoO_2) have been attracting great attention because of their interesting thermoelectric properties at high temperature applications.[1] The enhanced thermoelectric power and electrical conductivity in Co oxides is apparently due to spin and orbital degrees of freedom of Co^{4+} in the low-spin state.[1] With respect to electronic properties, mixed-valence Rh oxides (Rh^{3+} and Rh^{4+}) resemble mixed-valence cobalt oxides (Co^{3+} and Co^{4+}) as expected from their location in the periodic table. Hence, Rh oxides also should form materials with a large thermopower (Seebeck coefficient) coupled with high conductivity and make them potential candidates for high temperature thermoelectric materials for power generation.[1]

It is well-known that some transition metal oxides (e.g., manganese oxides) form open rutile-type octahedral framework structures with large channels occupied by large cations, hydroxyl groups, or water.[2,3] Recently, we reported various Rh oxides with channel structures: $(Bi_6O_5)Rh_{12}O_{24}$ (todorokite-type), $(Bi_{2/3},Ce_{1/3})Rh_2O_5$, and $(Ln_{1-y}Bi_y)_{2/3-x}Rh_2O_4$ ($CaFe_2O_4$-type).[4−6] In the $(Bi_6O_5)Rh_{12}O_{24}$ todorokite-type oxide, a $(Bi_6O_5)^{8+}$ chain is located within a $(Rh_{12}O_{24})^{8-}$ framework.[4,7] In fact, these oxides are very stable materials that can be made at high temperatures in air. This is in contrast to Mn todorokites, which are made by a low-temperature hydrothermal process.

The structure of $SrCa_2Sc_6O_{12}$ was reported by Muller-Buschbaum et al. in 1975.[8] Subsequently, the isostructural compounds $(Sr_{0.56}Ca_{1.11}Yb_{0.67})Yb_6O_{12}$, $BaSr_2Y_6O_{12}$, $BaSr_2Er_6O_{12}$, $BaSr_2Tm_6O_{12}$, $Ba_2SrYb_6O_{12}$, $Ba_2SrTm_6O_{12}$, $BaCa_2Y_6O_{12}$, $BaCa_2In_6O_{12}$, and $BaSr_2In_6O_{12}$ were also reported by Muller-Buschbaum et al.[9−13] More recently, high pressure has been used to prepare $(K,Na)_{0.9}(Mg,Fe)_2(Mg,Fe,Al,Si)_6O_{12}$, $CaMg_2Al_6O_{12}$, and $K_{0.82}Mg_{1.68}(Cr_{2.84}Fe_{0.84}Ti_{2.11}Zr_{0.08})O_{12}$ with the $SrCa_2Sc_6O_{12}$ structure.[14−16] There has been one report of Ru oxides with the $SrCa_2Sc_6O_{12}$ structure although these compounds were not recognized as having the $SrCa_2Sc_6O_{12}$ structure.[17] These are of the formula $ALi_2Ru_6O_{12}$ where A can be Na, K, Ca, or Sr. In this paper, we report on the synthesis and characterization of a new family of rhodium oxides with the $SrCa_2Sc_6O_{12}$ structure and the general formula $AA'_2Rh_6O_{12}$.

* To whom correspondence should be addressed. Fax: (541) 737-8235. E-mail: mas.subramanian@oregonstate.edu.
[†] Oregon State University.
[‡] DuPont Central Research and Development.

(1) Koumoto, K.; Terasaki, I.; Funahashi, R. *MRS Bull* **2006**, *31* (3), 206. [Tritt, T. M.; Subramanian, M. A., Eds.].
(2) Shen, Y. F.; Zerger, R. P.; DeGuzman, R. N.; Suib, S. L.; McCurdy, L.; Potter, D. I.; O'Young, C. L. *Science* **1993**, *260*, 511.
(3) Post, J. E. *Proc. Natl. Acad. Sci. U.S.A.* **1999**, *96*, 3447.
(4) Mizoguchi, H.; Marshall, W. J.; Ramirez, A. P.; Sleight, A. W.; Subramanian, M. A. *J. Solid State Chem.* **2007**, *180*, 3463.
(5) Mizoguchi, H.; Ramirez, A. P.; Zakharov, L. N.; Sleight, A. W.; Subramanian, M. A. *J. Solid State Chem.* **2008**, *181*, 56.
(6) Mizoguchi, H.; Zakharov, L. N.; Ramirez, A. P.; Marshall, W. J.; Sleight, A. W.; Subramanian, M. A. *Inorg. Chem.* **2009**, *48*, 204.
(7) Stowasser, F.; Renkenberger, C. *Z. Kristallogr.* **2006**, *221*, 206.
(8) Muller-Buschbaum, Hk.; Muschick, W. Z. *Anorg. Allgem. Chem.* **1975**, *412*, 209.
(9) Muschick, M.; Muller-Buschbaum, Hk. *Z. Naturforsch. B* **1976**, *31*, 1064.
(10) Schluze, A. R.; Muller-Buschbaum, Hk. *Z. Naturforsch. B* **1981**, *36*, 837.
(11) Kruger, J.; Muller-Buschbaum, Hk. *J. Less-Common Met.* **1985**, *109*, 37.
(12) Schroder, F.; Muller-Buschbaum, Hk. *J. Less-Common Met.* **1986**, *116*, 211.
(13) Lalla, A.; Muller-Buschbaum, Hk. *Z. Anorg. Allg. Chem.* **1988**, *563*, 11.
(14) Gasparik, T.; Tripathi, A.; Parise, J. B. *Am. Mineral.* **2000**, *85*, 613.
(15) Miura, H.; Hamada, Y.; Suzuki, T.; Akaogi, M.; Miyajima, N.; Fujino, K. *Am. Mineral.* **2000**, *85*, 1799.
(16) Yang, H.; Konzett, J. *J. Solid State Chem.* **2004**, *177*, 4576.
(17) Foo, M. L.; He, T.; Huang, Q.; Zandbergen, H. W.; Siegrist, T.; Lawes, G.; Ramirez, A. P.; Cava, R. J. *J. Solid State Chem.* **2006**, *179*, 941.

10.1021/cm803345s CCC: $40.75
Published on Web 02/20/2009

Table 1. Hexagonal Lattice Constants for AA′$_2$Rh$_6$O$_{12}$

	$SrMg_2Rh_6O_{12}$	$La_{1-x}Mg_{2-y}Rh_6O_{12}$	$SrBe_2Rh_6O_{12}$
a (Å)	9.2004(9)	9.183(1)	9.0155(7)
c (Å)	2.9581(3)	2.9615(3)	3.0170(2)

Experimental Section

Reactants were Bi_2O_3 (99.9% Baker), PbO (99.9% Aldrich), V_2O_5 (99.9%, Adrich), Li_2CO_3 (99.6%, Sigma), MgO (99%, Aldrich), $SrCO_3$ (99.9%, Aldrich), BeO(99%, Alfa Aesar), Sc_2O_3 (99.99%, Stanford Materials Corporation), La_2O_3 (99.999%, AlfaAesar), and Rh_2O_3 prepared from $RhCl_3 \cdot H_2O$(99.9%, Alfa Aesar) by heating in moist air at 1073 K for 10 h. La_2O_3 was also heated at 1273 K for 5 h, before weighing. Ignition-loss for MgO was corrected before weighing. Appropriate amounts of metal oxide/metal carbonate and Rh_2O_3 were mixed by grinding together under ethanol in an agate mortar and pestle. This pressed mixture was placed in an alumina boat and heated under O_2 at 1173 K for 20 h and 1273 K for 10 h with intermediate grinding.

X-ray powder diffraction patterns were obtained with a RIGAKU MINIFLEX II using Cu Kα radiation and a Ni filter. Unit-cell dimensions were refined using a LeBail fit. Obtained lattice constants for polycrystalline samples are given in Table 1.

Single crystals of $Bi_{0.75}Sc_{1.10}(Rh_{4.92}Sc_{1.08})O_{12}$, $Bi_{0.68}Be_2Rh_6O_{12}$, $Bi_{0.78}Li_2Rh_6O_{12}$, and $Pb_{0.78}Li_2Rh_6O_{12}$ were grown in 75%Bi_2O_3−25%V_2O_5 or PbO−50%V_2O_5 molten flux. The intimate mixtures of Sc_2O_3/Rh_2O_3, $5Li_2CO_3/Rh_2O_3$, and $2BeO/Rh_2O_3$ were added with a 4-fold excess by weight of flux for $Bi_{0.75}Sc_{1.10}(Rh_{4.92}Sc_{1.08})O_{12}$, $Bi_{0.78}Li_2Rh_6O_{12}/Pb_{0.78}Li_2Rh_6O_{12}$, and $Bi_{0.68}Be_2Rh_6O_{12}$, respectively. These were heated to 1373 K in air in a covered platinum or alumina crucible. After the mixtures were held at this temperature for 10 h, the crucible was cooled to 973 K at a rate of 5 K/h. After reaching 973 K, the crucible was cooled to room temperature at a rate of 200 K/h. The flux was dissolved in HNO_3 (aq) at 360 K. The products consisted of black shiny needle crystals 0.5−4 mm in length. Figure 1 shows a photograph of a $Bi_{0.8}Li_2Rh_6O_{12}$ single crystal.

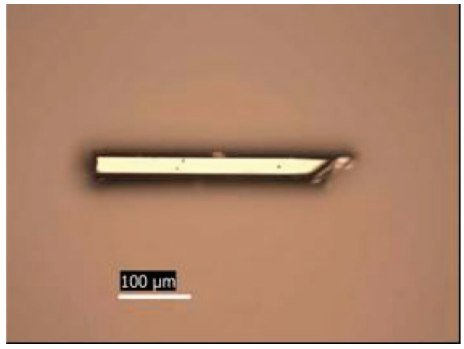

Figure 1. Photograph of a flux-grown single crystal of $Bi_{0.78}Li_2Rh_6O_{12}$.

Single-crystal X-ray diffraction data were collected using a Bruker SMART APEXII CCD system at 173 K. A standard focus tube was used with an anode power of 50 KV at 30 mA, a crystal to plate distance of 5.0 cm, 512 × 512 pixels/frame, beam center (256.52, 253.16), total frames of 6602, oscillation/frame of 0.50°, exposure/frame of 10.0 s/frame, and SAINT integration. A subsequent SADABS correction was applied. The crystal structure was solved with the direct method program SHELXS and refined with full-matrix least-squares program SHELXTL.[18] For refinement of occupation factors, the assumption was made that both the cation and anion sites of the MO_2 network were fully occupied. It was further assumed that Pb and Bi occupied only A sites and that Li, Sc, and Be ocupied only the A′ site. The M site was fully occupied by Rh except in the case of $Bi_{0.75}Sc_{1.10}(Rh_{4.92}Sc_{1.08})O_{12}$, where there was some Sc on this site.

DC electrical conductivities measurements were conducted by the conventional four-probe method (or two-probe method for lower conductivity samples) over the temperature region 80−300 K. Seebeck coefficient measurements were conducted over the temperature region 120−300 K. Magnetic measurements were made using a Quantum Design magnetic properties measurement system (MPMS).

Results

The new rhodium oxides with the $SrCa_2Sc_6O_{12}$ structure prepared in this study are $SrMg_2Rh_6O_{12}$, $La_{1-x}Mg_{2-y}Rh_6O_{12}$, $Bi_{0.78}Li_2Rh_6O_{12}$, $Pb_{0.78}Li_2Rh_6O_{12}$, $Bi_{0.75}Sc_{1.10}(Rh_{4.92}Sc_{1.08})O_{12}$, $SrBe_2Rh_6O_{12}$, and $Bi_{0.68}Be_2Rh_6O_{12}$. All pellets of these compounds were a bluish black color except for $SrMg_2Rh_6O_{12}$, which was dark brown. Attempts to obtain a pure phase in the $La_{1-x}Mg_{2-y}Rh_6O_{12}$ system failed. The impurity phases $LaRhO_3$ and/or $MgRh_2O_4$ were always observed in XRD patterns. However, these impurity peaks were very weak for a $La_{0.8}Mg_{1.8}Rh_6O_{12}$ composition. Single-crystal X-ray diffraction data were obtained for $Pb_{0.78}Li_2Rh_6O_{12}$, $Bi_{0.78}Li_2Rh_6O_{12}$, $Bi_{0.75}Sc_{1.10}(Rh_{4.92}Sc_{1.08})O_{12}$, and $Bi_{0.68}Be_2Rh_6O_{12}$. The formulas given for these crystals are based on refinement of occupation parameters. Results of the structural analyses are given in Tables 2 and 3, and in CIF files in the Supporting Information. The structures of $Bi_{0.78}Li_2Rh_6O_{12}$ and $Bi_{0.68}Be_2Rh_6O_{12}$ are shown in Figure 2. The coordination of the A′ cation is also shown in Figure 3. Some bond distances are given in Table 4. The longer M−O distances in the case of $Bi_{0.75}Sc_{1.10}(Rh_{4.92}Sc_{1.08})O_{12}$ are consistent with the partial substitution of Sc for Rh on this site.

Table 2. Crystallographic Information for AA′$_2$M$_6$O$_{12}$ Compounds; X-ray Data Were Collected at 173 K

	$Pb_{0.78}Li_2Rh_6O_{12}$	$Bi_{0.78}Li_2Rh_6O_{12}$	$Bi_{0.75}Sc_{1.10}(Rh_{4.92}Sc_{1.08})O_{12}$	$Bi_{0.68}Be_2Rh_6O_{12}$
fw	985.63	986.34	953.07	969.58
space group	*P6$_3$/m*	*P6$_3$/m*	*P6$_3$/m*	*P6$_3$/m*
a (Å)	9.129(4)	9.1263(2)	9.202(3)	8.9927(4)
c (Å)	2.985(3)	2.9899(1)	2.987(2)	3.0604(3)
V (Å^3)	215.5(2)	215.66(1)	219.1(2)	214.33(2)
Z	1	1	1	1
ρ_{calcd} (g cm^{-3})	6.345	7.595	7.224	7.512
μ (mm^{-1})	11.294	29.13	25.687	25.251
no of reflns measured	2686	11995	2540	2415
no. of reflns ind.	214 [R_{int} = 0.0236]	318 [R_{int} = 0.0156]	209 [R_{int} = 0.0207]	186 [R_{int} = 0.0325]
data/restraints/params	214/0/27	318/0/28	209/1/29	186/0/25
R_1/wR_2 [$I > 2\sigma(I)$]	0.0202/0.0432	0.0172/0.0412	0.0203/0.0527	0.0186/0.0573
R_1/wR_2 [all data]	0.0229/0.0454	0.0173/0.0413	0.0212/0.0540	0.0188/0.0574
GOF on F^2	1.11	1.19	1.28	1.03

Table 3. Atomic Coordinates and Displacement Factors for $AA'_2M_6O_{12}$ Compounds

		$Pb_{0.78}Li_2Rh_6O_{12}$	$Bi_{0.78}Li_2Rh_6O_{12}$	$Bi_{0.75}Sc_{1.10}(Rh_{4.92}Sc_{1.08})O_{12}$	$Bi_{0.68}Be_2Rh_6O_{12}$
M (6 h)	x	0.0211(1)	0.0218(1)	0.0222(1)	0.0288(1)
	y	0.3630(1)	0.3630(1)	0.3617(1)	0.3641(1)
	U(eq) (Å $\times$ 10^3)[a]	5(1)	5(1)	5(1)	3(1)
A1[b]	z	0.364(8)	0.309(1)	0.143(14)	
	U(eq) (Å $\times$ 10^3)	24(8)	12(1)	10(30)	25(1)
	occ.	0.08(3)	0.106(13)	0.187(2)	0.341(2)
A2[c]	z	−0.127(40)	−0.074(9)		
	U(eq) (Å $\times$ 10^3)	0.001(4)	10(1)		
	occ.	0.11(3)	0.089(13)		
A′[c]	U(eq) (Å $\times$ 10^3)	19(5)	34(4)	10(1)	10(3)
	occ.	1	1	0.551(10)	1
O1 (6 h)	x	0.1957(5)	0.1926(3)	0.1927(4)	0.1989(5)
	y	0.2903(5)	0.2842(3)	0.2838(5)	0.2818(5)
	U(eq) (Å $\times$ 10^3)	9(1)	8(1)	9(1)	6(1)
O2 (6 h)	x	0.8673(6)	0.8676(3)	0.8644(4)	0.8625(5)
	y	0.4649(5)	0.4644(3)	0.4606(4)	0.4592(5)
	U(eq) (Å $\times$ 10^3)	7(1)	7(1)	11(1)	5(1)

[a] U(eq) is defined as one-third of the trace of the orthogonalized U^{ij} tensor. [b] Split site model into two 4e sites (0, 0, z) is applied for the A sites of $Pb_{0.78}Li_2Rh_6O_{12}$ and $Bi_{0.78}Li_2Rh_6O_{12}$. The 4e and 2a sites are occupied for $Bi_{0.75}Sc_{1.10}(Rh_{4.92}Sc_{1.08})O_{12}$ and $Bi_{0.68}Be_2Rh_6O_{12}$, respectively. [c] The 2d site is occupied by Be for $Bi_{0.68}Be_2Rh_6O_{12}$.The 2c site is occupied by A′ ion for the other three compounds.

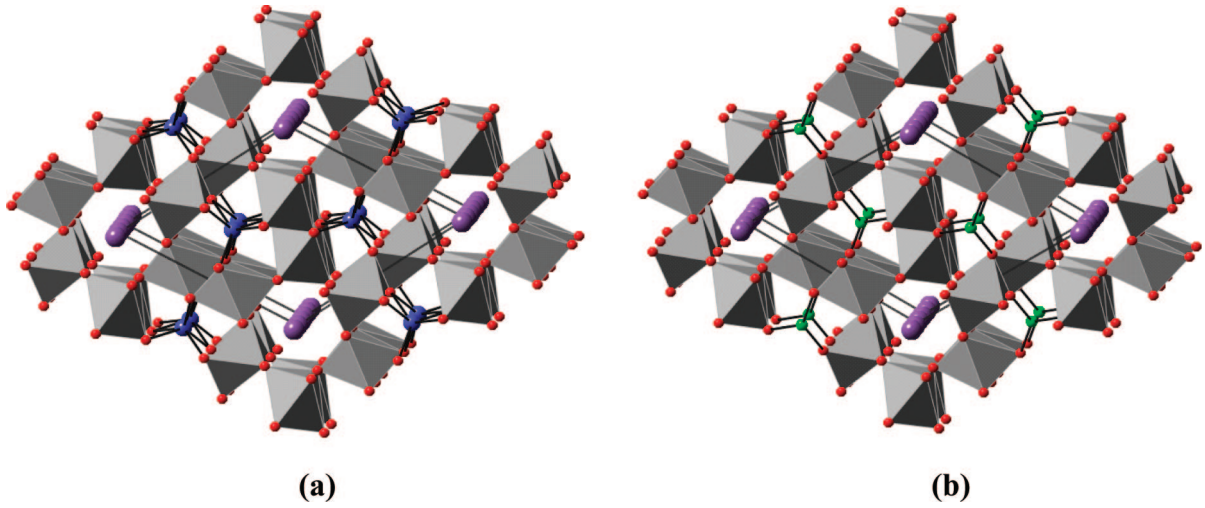

Figure 2. (a) Crystal structure of $Bi_{0.78}Li_2Rh_6O_{12}$. The Rh atoms are located within the octahedra. Oxygen atoms are shown as small red spheres. The Li atoms (blue) and Bi atoms (violet) reside in the tunnels. (b) Crystal structure of $Bi_{0.68}Be_2Rh_6O_{12}$ where the smaller channels are occupied with Be atoms (green) in triangular coordination.

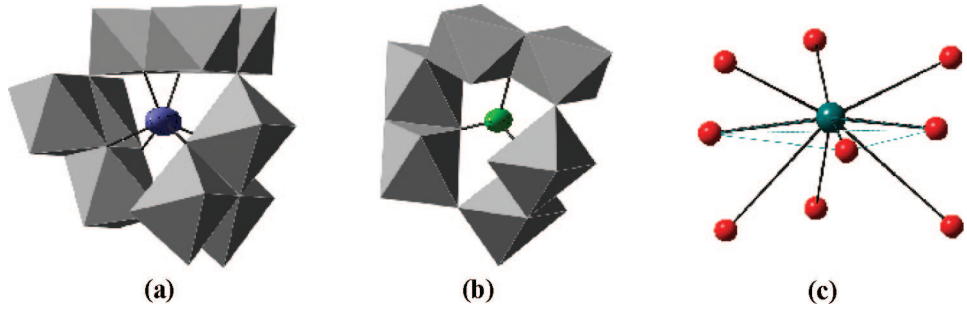

Figure 3. Coordination of the A′ cations in the tunnel for (a) $Bi_{0.78}Li_2Rh_6O_{12}$ and (b) $Bi_{0.68}Be_2Rh_6O_{12}$. RhO_6 octahedra are gray. (c) Coordination of Pb ion for $Pb_{0.78}Li_2Rh_6O_{12}$.

The temperature dependences of electrical conductivity and Seebeck coefficients are shown in panels a and b in Figure 4, respectively. The observed values of conductivity are in the range 1−200 Scm^{-1} and change very little with temperature. Both grain boundary resistance and pellet porosity may contribute to the lower conductivities of pellets relative to single crystals. However, the single-crystal measurements are only along the direction of the continuous edge shared chains, and conductivity may be higher in that direction than in direction perpendicular to the c axis. Although the brown color of the $SrMg_2Rh_6O_{12}$ pellet suggests a Rh valence close to 3+, good conductivity is observed. For $Bi_{0.68}Be_2Rh_6O_{12}$ needles, the conductivity at 300 K estimated by the two-probe method was low (5.1 $\times$ 10^{-2} S/cm), indicating that the Rh valence is very close to 3+. All the samples show positive Seebeck

Table 4. Selected Bond Distances (Å) for AA′$_2$M$_6$O$_{12}$ Compounds

	$Pb_{0.78}Li_2Rh_6O_{12}$	$Bi_{0.78}Li_2Rh_6O_{12}$	$Bi_{0.75}Sc_{1.10}(Rh_{4.92}Sc_{1.08})O_{12}$	$Bi_{0.68}Be_2Rh_6O_{12}$
M−O(1)	2.009(4)	2.017(2)	2.024(3)	2.005(4)
M−O(1) × 2	2.016(3)	2.0284(15)	2.029(2)	2.016(2)
M−O(2)	2.036(4)	2.035(2)	2.064(3)	2.061(4)
M−O(2) × 2	2.033(3)	2.0357(15)	2.070(3)	2.063(3)
M−M × 2[a]	2.985(3)	2.9899(1)	2.987(2)	3.0604(3)
M−M × 2[b]	3.0978(15)	3.1055(4)	3.1494(13)	3.1387(4)
A′−O(2) × 6	2.197(3)	2.1991(16)	2.187(3)	
A′−O(2) × 3				1.546(4)

[a] Perpendicular to the *ab* plane. [b] In the *ab* plane.

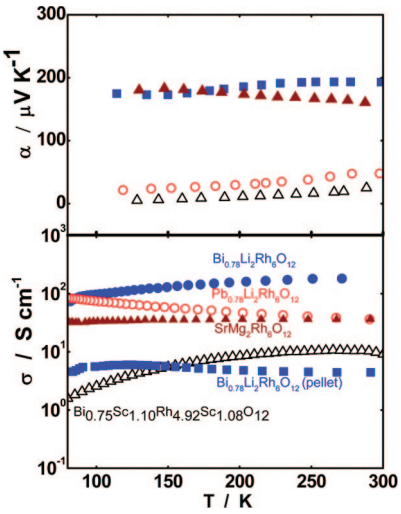

Figure 4. Temperature versus electrical conductivity (along the *c*-axis for single crystals) (bottom) and Seebeck coefficient (top) data for AA′$_2$Rh$_6$O$_{12}$ samples.

coefficients (Figure 4b) indicating majority of the charge carriers responsible for the conduction are holes. At 300 K, $Bi_{0.78}Li_2Rh_6O_{12}$ and $SrMg_2Rh_6O_{12}$ show large Seebeck coefficients and good electrical conductivity. The calculated power factors for thermoelectric conversion are 0.13 × 10^{-4} and 0.9 × 10^{-4} W m^{-1} K^{-2}, respectively, and are comparable to the values reported for *p*-type oxides containing Co (e.g., Na_xCoO_2, $Ca_3Co_4O_9$) and Rh (e.g., $CuRh_{1-x}Mg_xO_2$) at room temperature.[1]

Figure 7shows the temperature dependence of magnetic susceptibility per Rh atom for $Pb_{0.78}Li_2Rh_6O_{12}$, $Bi_{0.78}Li_2Rh_6O_{12}$, and $Bi_{0.68}Be_2Rh_6O_{12}$. Below 50 K, the susceptibilities increase sharply indicative of a localized magnetic moment (Curie−Weiss paramagnetism). Taking into consideration of the high electrical conductivities, a temperature-independent term (Pauli term) due to free carriers was included in the C−W formula $\chi_0 + C/(T - \theta)$ for the fitting. The obtained parameters are summarized in Table 5. The small and negative Weiss constants suggest very weak antiferromagnetic interaction between spins. Temperature-independent terms are 0.6 × 10^{-5} to 9 × 10^{-5} emu (mol Rh)$^{-1}$ and correspond to the density of states near E_F. These are approximately proportional to Rh valence, as shown in the inset of Figure 7.

Discussion

The structure of the compounds reported here is based on a RhO_2 framework with two kinds of channels. Other known structures based on a RhO_2 network are shown in Figure 5. In all four structures shown in Figures 2 and 5, there is continuous edge sharing of octahedra in the direction perpendicular to the plane shown. In both the $CaFe_2O_4$ and $SrCa_2Sc_6O_{12}$ structures, octahedra also share edges in pairs within the plane shown in Figures 2 and 5. In the $SrCa_2Sc_6O_{12}$ structure, all O atoms are bonded to three Rh atoms as is the case in rutile-type RhO_2, todorokite ($(Bi_6O_5)Rh_{12}O_{24}$), and $CaFe_2O_4$-type phases ($(R_{1-y}Bi_y)_{2/3-x}Rh_2O_4$), where *R* is a rare earth ion. Two rutile-chains running along the *c*-axis in the $SrCa_2Sc_6O_{12}$ structure share edges with each other, resulting in the formation of double rutile-chain. These double rutile-chains share corners with each other to form a RhO_2 framework. No Rh−Rh bonding is expected across the edge-shared octahedra in view of the nearly filled 4d t_{2g}* orbitals. This is confirmed by the Rh−Rh interatomic distances.

The formulas obtained from single-crystal X-ray diffraction analyses are $Pb_{0.78}Li_2Rh_6O_{12}$, $Bi_{0.78}Li_2Rh_6O_{12}$, $Bi_{0.75}Sc_{1.10}(Rh_{4.92}Sc_{1.08})O_{12}$, and $Bi_{0.68}Be_2Rh_6O_{12}$. These formulas indicate Rh oxidation states of 3.4, 3.3, 3.1, and 3.0, respectively for these four compounds. The average Rh−O distance is expected to decrease as the average oxidation state of Rh increases, and this is consistent with the Rh−O distances found in $Bi_{0.68}Be_2Rh_6O_{12}$ (2.037 Å), $Bi_{0.78}Li_2Rh_6O_{12}$ (2.030 Å), and $Pb_{0.78}Li_2Rh_6O_{12}$ (2.024 Å).

The A′ cations in the smaller of the two channels of the $SrCa_2Sc_6O_{12}$ structure normally occupy sites with trigonal prismatic coordination. This is also the case for our new compounds, except in the case of $Bi_{0.68}Be_2Rh_6O_{12}$ (and presumably $SrBe_2Rh_6O_{12}$), where Be is in triangular coordination. These compounds are the first examples of Be in the $SrCa_2Sc_6O_{12}$ structure and the first examples of the A′ cation occupying the triangular sites in the small channels. However, the mineral $BMg_3(OH,F)_6$ has essentially the same structure as $Bi_{0.68}Be_2Rh_6O_{12}$, except that in $BMg_3(OH,F)_6$, the B atoms occupy the triangular sites and Mg atoms occupy the octahedral sites.[19] There are no A cations in the large channels of $BMg_3(OH,F)_6$, but these channels may have some H atoms from OH^- groups and possibly some H_2O as well. The Be−O distance of 1.546 Å that we find in $Bi_{0.68}Be_2Rh_6O_{12}$ is precisely that expected on the basis of ionic radii.[20] However, to achieve this distance, there is a

(18) Sheldrick, G. M. *SHELXTL*, version 6.14; Bruker Analytical X-ray Instruments, Inc.: Madison, WI, 2003.

(19) Takeuchi, Y. *Acta Crystallogr.* **1950**, *3*, 208.

(20) Shannon, R. D. *Acta Crystallogr., Sect. B* **1970**, *26*, 447.

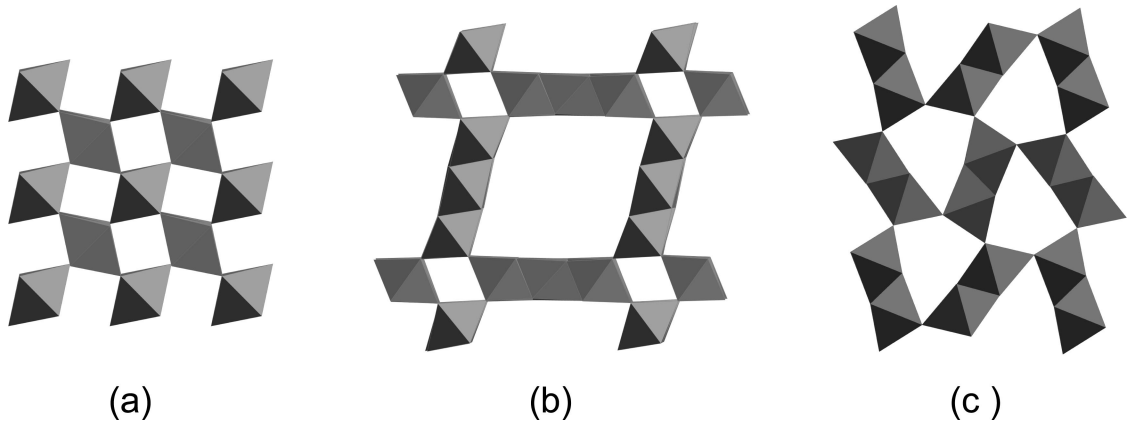

Figure 5. MO_2 networks in (a) rutile, (b) todorokite, and (c) $CaFe_2O_4$-type are shown. In all cases, the octahedra share edges to form chains in the third direction.

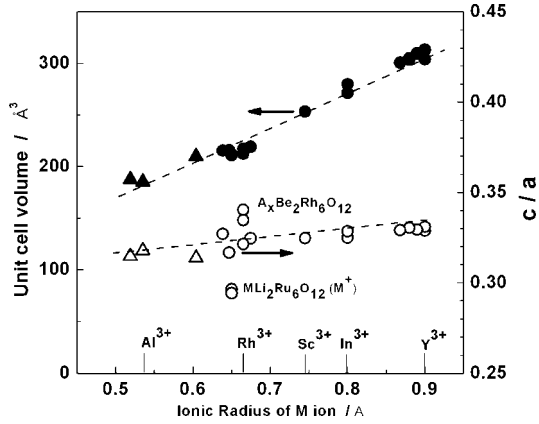

Figure 6. Unit-cell volume and *c*/*a* ratio versus ionic radius[20] of the octahedral M cation for $AA'_2M_6O_{12}$ family (circles). The oxides synthesized under high pressure are shown as triangles.

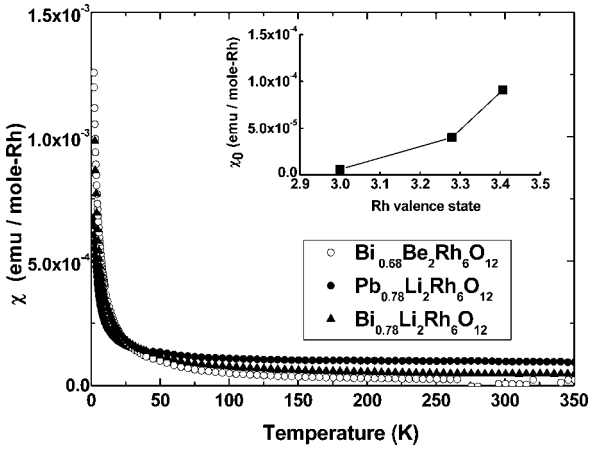

Figure 7. Magnetic susceptibility of $AA'_2Rh_6O_{12}$ pellets obtained under 0.5 or 1.0 T. The inset shows the Rh-valence dependence of the temperature-independent term of the fitting.

contraction of the *a* and *b* cell edges in both $Bi_{0.68}Be_2Rh_6O_{12}$ and $SrBe_2Rh_6O_{12}$ relative to other rhodates with this structure.

The number of large channels in the $SrCa_2Sc_6O_{12}$ structure is half the number of small channels, and the situation in these larger channels is complex. There are three sites available in the center of this larger channel (2a, 2b, and 4e). For the ideal $AA'_2M_6O_{12}$ formula, the number of A atoms is only half that required to fill either the 2a or the 2b sites. Furthermore, neither the 2a nor the 2b sites could be fully occupied because the A atoms would then be less than 1.5 Å apart. Atoms placed in the 4e site would be even closer together if this site were fully occupied. The usual situation for compounds reported with the $SrCa_2Sc_6O_{12}$ structure is that half of the 2a sites are occupied with A cations. In all four of our single-crystal diffraction studies, refinement of the thermal ellipsoid of the A cation placed in the 2a site became very elongated along the *c* axis, indicating large static displacements from the 2a site. In the case of $Pb_{0.78}Li_2Rh_6O_{12}$, the position of Pb using the 4e site refined as being displaced 0.37 Å above or below the ideal 2a site, as shown in Figure 3. An A cation in the 2a site would be in the center of the oxygen triangle shown. The two oxygen triangles above and below then give a total coordination of nine for the A cation. In the case of $Bi_{0.78}Li_2Rh_6O_{12}$, the Bi atom was placed in two different 4e sites to simulate the disorder of Bi along the *c* axis. The occupied and unoccupied A sites cannot be ordered without developing a superstructure along the *c* axis. A superstructure that could indicate A cation ordering has been reported only for $NaLi_2Ru_6O_{12}$ and $(Ba_{0.85}Ca_{0.15})Ca_2In_6O_{12}$.[17,21] We find no evidence for such a superstructure for the new compounds we are reporting. If charge ordering of Rh occurred, this would most likely lead to a superstructure along the *c* axis. Charge ordering of mixed-valence Rh is not common but has been observed in $Ln_{18}Li_8Rh_5O_{39}$ compounds where Ln can be La or Pr and in $(Bi_6O_5)Rh_4^{3+}Rh_8^{3.5+}O_{24}$.[4,22] The disorder of the A cations in our $AA'_2Rh_6O_{12}$ phases may inhibit charge ordering of Rh.

Table 5. Fitting Parameters to the Curie−Weiss Formula with a Temperature-ndependent Term (χ_0)

	$Pb_{0.78}Li_2Rh_6O_{12}$	$Bi_{0.78}Li_2Rh_6O_{12}$	$Bi_{0.68}Be_2Rh_6O_{12}$
χ_0 (emu (mol Rh)$^{-1}$)	9.1×10^{-5}	4.0×10^{-5}	0.6×10^{-5}
θ (K)	−1.1	−1.3	−1.6
C (emu K^{-1} (mol Rh)$^{-1}$)	0.0018	0.0035	0.0045
μ_{eff}	0.12 μ_B	0.17 μ_B	0.19 μ_B
temp range (K)	2−350	2−350	2−260

Figure 6 shows the relation between unit cell volume and the ionic radius of the octahedral M cation.[20] The trend is very good considering that the sizes and amounts of the A and A′ cations are ignored. The *c*/*a* ratio vs the ionic radius

(21) Jaldinozzi, G.; Goutenoire, F.; Hervieu, M.; Suard, E.; Grebille, D. *Acta Crystallogr., Sect. B* **1996**, *52*, 780.
(22) Frampton, P. P. C.; Battle, P. D.; Ritter, C. *Inorg. Chem.* **2005**, *44*, 7138.

of M is also shown in Figure 6. Again, there is a smooth trend except when M is Ru. Comparing the compounds where M is Rh or Ru, *c*/*a* decreases as the filling of the t_{2g} band decreases. When this band is completely occupied, as it is for Rh^{3+}, the interaction of the Rh 4d orbitals across the shared octahedral edges is strongly antibonding. Thus, the Rh atoms are repelled from each other for this reason as well as from the electrostatic repulsion of two 3+ cations. The Rh−Rh distances perpendicular to the *c* axis can simply increase in response to this situation. This is not an option for the Rh−Rh distances along the *c* axis because moving a Rh atom away from one its neighbors would move it toward another Rh atom. Thus, the Rh−Rh distances along the *c* axis are shorter than those perpendicular to the *c* axis (Table 4). When holes are introduced into the t_{2g} band, they will tend localize on orbitals pointing along the *c* axis because this will decrease the antibonding interaction between the Rh or Ru atoms that are closest to one another. In fact, the antibonding interaction becomes a bonding interaction. This tendency to localize the holes will in turn cause the *c*/*a* ratio to decrease. Thus, there is a large drop in *c*/*a* on going from the nearly filled t_{2g}* band of our rhodates to the 75% filled band for $ALi_2Ru_6O_{12}$ compounds where A is Na or K. The somewhat high *c*/*a* values for our Be rhodates relative to other rhodates is primarily due to the contraction of the *a* and *b* cell edges to achieve the appropriate Be−O distances.

Oxides of Rh^{3+} are semiconductors as expected for a filled t_{2g} band. They can be doped p- and n-type, and resistivities greater than 1×10^5 ohm cm are reported.[23] In oxides of Rh^{4+} the t_{2g} band is only 83% occupied, and good metallic properties might be expected. However, oxides of Rh^{4+} typically show properties intermediate between those of a good metal and a semiconductor. For example, $Sr_2Rh^{4+}O_4$ shows a nearly temperature independent electrical conductivity of about 10 S/cm.[24] Likewise, the magnetic behavior for $Sr_2Rh^{4+}O_4$ is intermediate between Pauli paramagnetism and that expected for a localized d electrons. Consequently, we do not expect that oxides containing mixed Rh^{3+} and Rh^{4+} will show good metallic properties. We find conductivities much higher than that expected for a pure Rh^{3+} situation. This and the p-type behavior confirm that some Rh^{4+} is present in all of our compounds. The temperature dependence of the conductivity for our compounds is weak as it is even in the case of $Sr_2Rh^{4+}O_4$.[24] The high Seebeck coefficients coupled with the high electrical conductivity make some of these compounds potential candidates as high-temperature thermoelectric materials for power generation.

Acknowledgment. We thank A. P. Ramirez (Bell Laboratories) for magnetic measurements. The work at Oregon State University is supported by grants from National Science Foundation (DMR 0804167) and Air Force Research Laboratory (FA8650-05-1-5041).

Supporting Information Available: Crystallographic details in CIF format. This material is available free of charge via the Internet at http://pubs.acs.org.

CM803345S

(23) Jarrett, H. S.; Sleight, A. W.; Kung, H. H.; Gilson, J. L. *J. Appl. Phys.* **1980**, *51*, 3916.

(24) Yamaura, K.; Huang, Q.; Young, D. P.; Takayama-Muromachi, E. *Chem. Mater.* **2004**, *16*, 3424.